Pergamon

Acta Materialia 50 (2002) 1771–1779

Acta MATERIALIA

www.actamat-journals.com

Strain tensor development in a single grain in the bulk of a polycrystal under loading

L. Margulies [a, b], T. Lorentzen [a], H.F. Poulsen [a,*], T. Leffers [a]

[a] *Materials Research Department, Risø National Laboratory, Roskilde 4000, Denmark*
[b] *ESRF, BP 220, F-38043 Grenoble Cedex, France*

Received 29 August 2001; received in revised form 28 December 2001; accepted 28 December 2001

Abstract

First results are presented on the development of the elastic strain tensor in a single embedded grain during tensile loading of a copper sample. The technique is based on the use of focused high-energy X-rays from a synchrotron source. Measurements are performed by the rotation method, and automated indexing routines are used to group reflections belonging to a single grain. In total, 17 reflections were monitored as a function of tensile load. At each load level three elements of the strain tensor were fitted using a singular value decomposition routine for over-determined linear systems. Sources of systematic error are discussed, and a method for extending the technique towards simultaneous measurements of ensembles of grains is outlined. © 2002 Published by Elsevier Science Ltd on behalf of Acta Materialia Inc.

Keywords: Stress–strain relationship measurements; X-ray diffraction

1. Introduction

The plastic deformation of polycrystals and the possibility of modelling this plastic deformation are of great technological importance, as almost all materials used for structural components are polycrystalline.

The first generation of polycrystal models—ranging from the relatively simple Sachs [1] and Taylor [2] models of the early part of the twentieth century to the relaxed–constraint models [3–5] to the more complex self-consistent models of the last part of the twentieth century (e.g. [6–10])—are all "one-site models" [9]. These consider the interaction of individual grains with some kind of continuum matrix, which means that all grains with the same crystallographic orientation behave in the same way. The next generation of polycrystal models, which have appeared in the last decade, are "*n*-site models" [9]. These consider the interaction of neighbouring grains, taking into account their specific crystallographic orientations. In practice, they are based on finite-element modelling (FEM), e.g. [11–14]. In these models all grains with the same crystallographic orientation do not behave in the same way.

The experimental evaluation of the different

* Corresponding author. Tel.: +45-4677-5739; fax: +45-4677-5758.
E-mail address: henning.friis.poulsen@risoe.dk (H.F. Poulsen).

1359-6454/02/$22.00
PII: S1359-6454(02)00028-9

polycrystal models obviously relies on comparison of various parameters derived from the models with experimental measurements of these parameters. Typical examples of such parameters are the flow stress, the texture and the strain heterogeneities, particularly their change with increasing strain. With the fairly recent introduction of neutron and hard X-ray diffraction, intergranular stresses have been added to the list of parameters. It is an unavoidable consequence of any reasonable polycrystal model that intergranular stresses develop, as reflected in lattice strains (type-2 internal stresses), e.g. [15–18]. These intergranular stresses are of great scientific and practical significance because (i) as already mentioned they may be used to evaluate the different polycrystal models, e.g. [16–18], and (ii) they are essential for the derivation of the macroscopic internal/residual stresses (type-1 stresses) from diffraction measurements of lattice strains, e.g. [17,19,20].

For one-site models, where all grains with the same crystallographic orientation behave in the same way, the natural experimental reference is "statistical" measurements of bulk lattice strains, traditionally performed by neutron diffraction. (The lattice strains in surface grains as measured by soft X-rays are irrelevant in this connection because they are not representative of the polycrystal.) Such diffraction measurements provide the average lattice strains in different populations of grains with specific lattice orientations, e.g. [15–22].

In contrast, the relevant experimental references for *n*-site models are measurements of lattice strains in individual grains. In the present work we demonstrate the feasibility of such in situ measurements of lattice strains in an embedded grain by diffraction with hard X-rays from a synchrotron. We continue to derive the dynamics of components of the strain tensor from the lattice-strain measurements. The actual measurements refer to purely elastic deformation, so they cannot be used for studying polycrystal plasticity. However, when we can measure the lattice strains in individual grains connected to elastic deformation, we can also measure the lattice strains connected to plastic deformation.

2. Basic approach

In order to derive bulk lattice strains we must use a type of radiation that can penetrate several grain diameters into the material. Furthermore, to enable the use of conventional deformation tools and avoid surface effects such as friction layers, a penetration of 1 mm is desirable. Neutrons meet this requirement, but the flux of currently available neutron sources is insufficient to provide the spatial resolution needed for the investigation of individual grains. Instead, we use the hard X-rays from a third-generation synchrotron source, in our case the ESRF in Grenoble. These sources provide the necessary combination of high penetration and high flux [23–25].

The beam of hard X-rays is focused onto a spot with dimensions slightly larger than the grain size. This beam simultaneously probes all the illuminated grains through the thickness of the sample, provided these are in a diffraction condition. In order to probe all the grains and for each of them to characterize a sufficient number of strain components to facilitate the calculation of the strain tensor, several sample orientations are required at each load level. The challenge is therefore:

(i) to sort the multitude of reflections with respect to grain of origin (this task can be performed by the recently established indexing program GRAINDEX, reported elsewhere [26]);
(ii) for each grain to accurately assess the lattice strain of the associated reflections;
(iii) to derive a strain tensor from the lattice strains;
(iv) to provide the necessary stability and alignment accuracy to study the variation in the strain tensors as a function of deformation.

In this presentation we focus on tasks (ii)–(iv), as the indexing program already has been used in various contexts and is able to index up to several hundred grains at the same time [27–29]. Hence, we will only deduce the strain tensor elements for one embedded grain. Furthermore, due to a restriction in the geometry of the particular set-up used for this feasibility test we will only derive the dynamics of three of the six tensor elements.

3. Experimental procedure

The experiment took place at the 3D X-ray diffraction microscope at beamline ID11 at ESRF. The microscope is dedicated to structural investigations in 3D, operating in the 50–100 keV regime with a spatial resolution down to 1.5×5×50 μm^3 [24]. A bent Laue monochromator was used to focus the beam vertically to 50 μm. The energy was 79.9 keV (0.155 Å wavelength), corresponding to a penetration depth in Cu of 1.5 mm. The divergence of the beam and the energy bandwidth were 0.3 mrad and 0.5%, respectively. Horizontally, the beam was defined to a width of 400 μm by a slit in front of the sample.

A sketch of the experimental set-up is given in Fig. 1. The sample tower consists of two translations (x,y) fixed on a rotation unit (ω), which is fixed on a vertical z-translation. The sample is mounted in a 25 kN Instron stress-rig on top of this tower, with the tensile axis pointing transversely to the beam for ω=0. The monochromatic beam defines a layer in the sample, fixed during the experiment. The diffracted beam from grains within this layer fulfils the scattering condition giving rise to spots on an area detector (transmission geometry). The detector is an image intensifier coupled to a CCD with an effective pixel size of 175 μm and an active area of 185×185 mm. The point-spread function was found to be of a pseudo-Voigt type with large tails, allowing fits spanning 7 pixels to be made. The detector was placed at a distance of 520 mm from the sample.

Measurements are performed by the "rotation-method" [26,27]; that is by acquiring images while stepping in ω with equidistant steps of $\Delta\omega$. During each acquisition the sample is oscillated by $\pm\Delta\omega/2$ in order to perform a space-filling and intensity-conserving sampling. Space constraints at the instrument dictated the ω-span to be 30°, while $\Delta\omega$ was set at 2°.

The sample was a well-annealed Cu specimen with dimensions 3×8×50 mm^3. It was mounted with the normal of the thin side parallel to the beam. The average grain size was 250 μm—that is smaller than the beam width. As illustrated in Fig. 2 this implies that at each ω-setting several grains are fully illuminated. The fact that several grains may give rise to spots on the two-dimensional detector complicates the analysis. As illustrated in Fig. 2a, diffraction from a grain, which is not well aligned over the centre of rotation gives rise to a radial displacement on the detector plane, which is subsequently converted into an erroneous d-spacing and an erroneous lattice strain. Moreover, if we do not assure grains to be well aligned over the centre of rotation, then each image acquired during the ω-scanning will render erroneous strain measures as the grain precesses around the centre of rotation. This is illustrated in

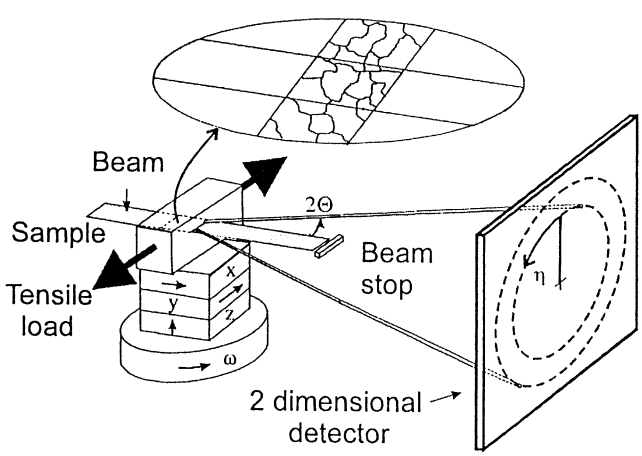

Fig. 1. Sketch of the experimental configuration with the stress-rig mounted on the sample table of the 3D X-ray microscope at the ID-11 beam line at the ESRF synchrotron source.

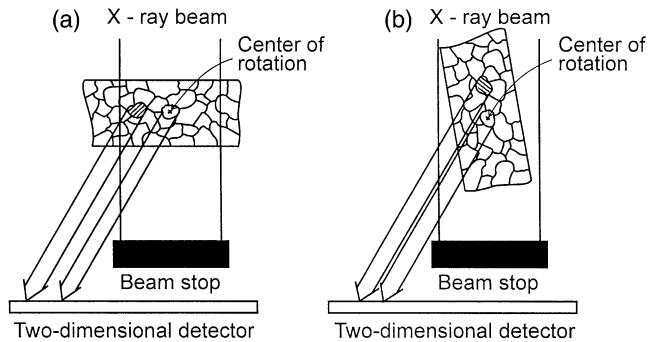

Fig. 2. The beam path through the sample illuminates all parts of the microstructure along the way. (a) Grains misplaced from the centre of rotation give rise to radial displacement of the diffraction spot on the detector plane, and hence result in an erroneous measurement of the diffraction angle, the d-spacing and the strain. (b) Grains not aligned over the centre of rotation will moreover give rise to erroneous measurements as the sample is rotated during the ω-scan.

Fig. 2b, where the sample is rotated in ω. During the ω-scanning we may even run the risk that grains at a distance from the axis of rotation will rotate partly or fully out of the illuminated area. This gives rise to apparent changes in the centre-of-mass (CMS) position of the spots on the detector, and subsequently gives rise to erroneous strain measurements.

Furthermore, during tensile loading the sample elongates and the position of any grain changes with respect to the rotation axis. To avoid erroneous strain determinations it is necessary to know where the CMS position is with respect to the axis. This can be measured experimentally at each load level—most elegantly by an X-ray tracing algorithm [26–28]—or the position can be fitted afterwards simultaneously with the strain. Here, the simpler approach is taken of only looking at one grain, and aligning that with respect to the rotation axis after each load increment.

The grain was aligned by acquiring images while stepping with the stress-rig along *y*. The integrated intensity of a spot from the grain of interest was calculated as a function of translation and the sample positioned according to the centre position. The accuracy of this alignment is estimated to be 5 μm.

The major error-source was predicted to be the stability of the sample position along *x* and drifts in beam energy. In order to monitor sample or beam movements on-line, a capillary was clamped to the top of the sample, containing a powder, identical in composition to the polycrystalline sample itself. The reference powder was also used for an initial alignment of the grain along *x*, as it was mounted symmetrically with respect to the sample. By triangulation with the beam, the centre of the capillary—and thereby the centre of the sample—was placed on top of the rotation axis.

The measuring procedure was as follows: the tensile load was changed, the grain aligned in the *y* direction, the sample translated in *z* to acquire an image of the reference powder at ω=0, the *z*-translation reversed and the ω-scan performed. At the end another image was acquired of the reference powder. This procedure was repeated seven times with increments in load of 0.2 kN, starting at 0 kN. The specimen was then unloaded, and a final round of measurements carried out. The ramping between levels took 60 seconds, and was performed with almost no overshoot.

The sample was loaded through two successive cycles, and the results presented here originate from the second cycle. This means that in this demonstration of the analysis principles we are not sensitive to irregular stress/strain paths at the lowest load levels of the initial cycle, and we operate on a loading sequence which is sound from the early stage. Moreover, we operate on a data set where the grain considered is preloaded at zero applied load with the residual intergranular strains developed during previous plastic deformation of the aggregate. We focus on the additional purely elastic loading in the second cycle.

The loading sequence was performed as an incremental step loading, maintaining a fixed applied load during the time it took to acquire the detector images associated with each ω-scan.

4. Data analysis procedure

In total, approximately 900 reflections occurred over the complete measurement range. Spatial distortion corrections were performed on the initial zero load data set using the software package FIT2D [30]. The spatially corrected data were then used as input to GRAINDEX [26]. From the resulting list of grains, one grain was selected, which was associated with 17 reflections. These formed a complete and self-consistent set with angular differences between calculated and measured positions of the spots of less than 0.5°. GRAINDEX also provided the orientation of this undeformed grain:

$$U = \begin{Bmatrix} -0.056 & -0.507 & -0.860 \\ 0.998 & -0.017 & 0.054 \\ 0.012 & 0.869 & 0.507 \end{Bmatrix} \quad (1)$$

using the definition $\boldsymbol{G}_s = U\boldsymbol{G}_c$, where $\boldsymbol{G}_c$ is the scattering vector with respect to the grain axes {[100], [010], [001]}, and $\boldsymbol{G}_s$ is the corresponding scattering vector with respect to the sample axes (ND_H, TD, ND_V). Here TD is the tensile direction and ND_H and ND_V are the transverse directions in the horizontal and vertical planes, respectively. Hence, within a few degrees, the grain has the <100> direction aligned parallel to the tensile direction.

The radial position of each reflection was extracted from the original images, without applying the spatial distortion correction. The spatial correction effectively redistributes the intensity of each reflection on the detector, and can produce artificial shifts in both the centre of mass and peak shape. As lattice strains were measured from the relative shifts of individual reflections, long-range detector distortions could be neglected and artificial shifts avoided due to the correction procedure. The radial position of each reflection was determined as follows. Each image was transformed to polar co-ordinates and a 5° azimuthal range (a 5° η interval, see Fig. 1) around each spot was integrated. Reflections that were spread across multiple images were summed before integration. The final radial profile was then fit to a pseudo-Voigt peak shape function. This procedure was followed for all 17 reflections at each load level. The peak shape was found to be dominated by instrumental broadening (the detector point spread function) and as such did not vary with reflection order or load level. In addition, for each reflection the corresponding azimuthal range of each standard powder pattern was similarly integrated and fitted. This was done in order to correct for small changes in the sample to detector distance, which occur during loading. Normalizing to the initial zero strain measurements, all shifts in the radial reflection positions were measured relative to the corresponding powder reflection positions at each strain level. The result is an accurate measure of the evolution of the lattice strain in the 17 reflections all originating from the same embedded grain. The results are shown in Fig. 3.

It is observed from Fig. 3 that the initial strain varies considerably among the 17 reflections with some showing tensile and some compression initial strains. Recall that the data originate from the second loop of the loading sequence, and hence the initial strains are residual intergranular strains caused by previous plastic deformation. Note also that some reflections develop increasingly higher lattice strains under loading, while for some the lattice strain is reduced. This is a natural consequence of the differences in orientations, with some reflections monitoring a longitudinal strain component, some monitoring a transverse component and some monitoring strain in a specific direction in between these sample directions.

With our recording of the orientation of the grain under consideration, we may now associate each of these curves of lattice strain evolution with a specific sample direction, and then proceed to a calculation of the strain tensor components.

4.1. Strain tensor derivation

Using diffraction, the basic equation for stress/strain determination is based on measure-

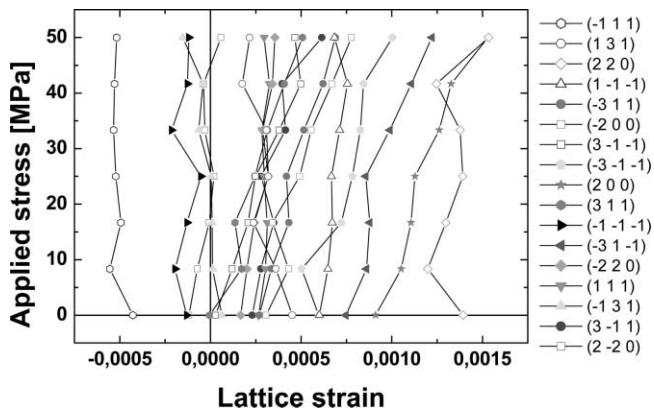

Fig. 3. Lattice strain evolution during the second loading cycle of the 17 available *hkl*-reflections for one embedded grain.

ments of relative changes in the d-spacing of selected lattice planes. The expression for a given strain component is found by differentiation of Bragg's law:

$$\varepsilon = \frac{d-d_0}{d_0} = -\cot(\theta)\,\Delta\theta. \tag{2}$$

In terms of a specific strain component ε_i in the direction identified by the direction cosines l_i, m_i and n_i, the expression can be written in matrix form as:

$$\varepsilon_i = (l_i \;\; m_i \;\; n_i)\begin{pmatrix} \varepsilon_{11} & \varepsilon_{12} & \varepsilon_{13} \\ \varepsilon_{12} & \varepsilon_{22} & \varepsilon_{23} \\ \varepsilon_{13} & \varepsilon_{23} & \varepsilon_{33} \end{pmatrix}\begin{pmatrix} l_i \\ m_i \\ n_i \end{pmatrix} \tag{3}$$

From this formalism we can express the strain in any direction given by l, m and n as a function of the components of the strain tensor in the coordinate system which the direction cosines refer to:

$$\varepsilon = \varepsilon_{11}l^2 + \varepsilon_{22}m^2 + \varepsilon_{33}n^2 + \varepsilon_{12}lm + \varepsilon_{13}\ln + \varepsilon_{23}mn \tag{4}$$

With six unknown components of the strain tensor, we require six independent measurements of ε to solve the linear set of equations. In reality, a surplus of measurements is required to compensate for the evident inaccuracy in measuring individual strain components; typically at least 10–12 measurements are required to prevent the errors in the strain tensor components to grow unacceptably large. Here we monitor 17 independent *hkl*-reflections, which means we accumulate sufficient information to render an over-determined system of equations, which is easily solved by singular value decomposition—an elegant and robust algorithm specifically suited for this purpose [31]. The results for the ε_{22}, ε_{33} and ε_{23} strain components as a function of applied load are given in Table 1. As mentioned, due to space constraints the experiment covered a rather narrow ω-range around 0°. This implies that we essentially probe the plane perpendicular to the specimen normal. Hence, the ε_{11} component and the related shear components ε_{12} and ε_{13} have large experimental errors. In order to adequately sample all six strain tensor components, it is necessary to collect data over a larger omega range, such as $-45°$ to 45°.

In Fig. 4 the three components from Table 1 are

Table 1
Strain tensor components calculated from a singular value decomposition fit to 17 independent reflections. Values are given in units of microstrain ($\times 10^{-6}$)

Applied load (MPa)	ε_{22}	ε_{33}	ε_{23}
0.0	770	131	332
8.0	849	7	267
16.7	918	38	269
25.0	911	39	342
33.3	1014	−91	289
41.7	1089	−111	251
50.0	1284	−187	337

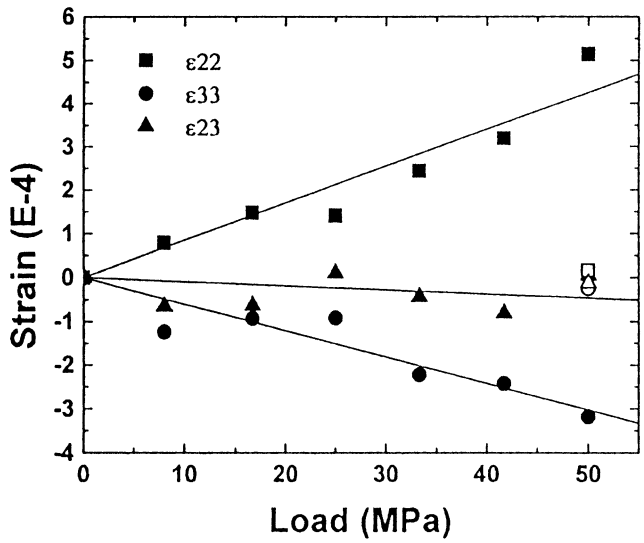

Fig. 4. The strain evolution as a function of load for the longitudinal ε_{22}(■) and transverse ε_{33}(●) normal components and the associated shear ε_{23}(▲) component of the strain tensor. Lines are linear fits to the experimental data points. Values after unloading are shown as unfilled symbols.

plotted with starting point zero for zero load (thus eliminating the residual strains introduced in the first, plastic loading cycle). The points for the three strain components lie approximately on three straight lines: one with a positive slope for the normal strain in the tensile direction, one with a smaller, negative slope for the normal strain in the x_3 transverse direction and one with a slope close to zero for the ε_{23} shear strain. Linear fits are included in the figure. The apparent *E*-modulus determined in this way (applied stress divided by longitudinal strain) is 113.5±13.9 GPa, to be compared with the diffraction elastic constant for the {200} reflection, 101.5 GPa [17], which would be the self-consistent solution (assuming that all <100> grains have identical behaviour).

The three points representing the strain components after unloading have been added to Fig. 4. The strains are seen to go back to zero with an accuracy of order 0.3×10^{-4}. In total, the results validate the experimental method and allow us to estimate the strain accuracy to be of order 10^{-4}.

5. Discussion

As demonstrated in Fig. 4 our measuring scheme and the subsequent data processing work as intended: we can determine the strain tensor—in our case three components of it—in an individual grain in the bulk. Strain development at the individual grain level should provide useful input and verification for the next generation of deformation models. In order for these data to be statistically relevant, large populations of grains, of the order of 100 to 1000, must be measured. This can, in principle, be done by centring a large number of grains and following each of them in a way identical to the procedure described here. However, it would be much more efficient to make use of the inherent property of GRAINDEX to index many grains simultaneously.

To perform simultaneous experiments in this way, we have to find a substitute for centring each grain—that is, another way of determining each grain's offset from the centre of rotation. This can be done in several ways. One way is to perform a complete 3D mapping of the grains prior to deformation, as described in the publication by Lauridsen et al. [26]. An experimentally simpler approach is to include the deviations (Δx,Δy) of each grain from the centre of rotation as additional parameters in the fitting routine. In this case Eq. (2) is modified as:

$$\varepsilon_i = (l_i \;\; m_i \;\; n_i)\begin{pmatrix} \varepsilon_{11} & \varepsilon_{12} & \varepsilon_{13} \\ \varepsilon_{12} & \varepsilon_{22} & \varepsilon_{23} \\ \varepsilon_{13} & \varepsilon_{23} & \varepsilon_{33} \end{pmatrix}\begin{pmatrix} l_i \\ m_i \\ n_i \end{pmatrix} - \left[\cos(\omega_i) + \frac{\sin(\omega_i)\sin(\eta_i)}{\tan(\theta_i)}\right]\frac{\Delta x}{L} - \left[\sin(\omega_i) + \frac{\cos(\omega_i)\sin(\eta_i)}{\tan(\theta_i)}\right]\frac{\Delta y}{L} \quad (5)$$

where Δx and Δy are the offsets in the sample system from the centre of rotation and L is the sample to detector distance. This equation can still be solved using the single value decomposition method, and the additional parameters, Δx and Δy, should be reasonably fitted as long as the ω range is sufficiently large to give suitable projections along both of these directions within the sample frame. Using this approach, a rough alignment of only one grain is needed at each load step to ensure that the same gauge volume is probed at each load level. It is then possible to obtain information on a statistical ensemble of grains within a realistic time frame. Such information may prove critical for developing realistic models of deformation behaviour that explicitly take into account stress/strain development at the individual grain level.

6. Conclusion

We have shown that we can derive elements of the strain tensor in a single embedded grain in a polycrystal by in situ synchrotron measurements of lattice strains. In combination with the inherent properties of the GRAINDEX algorithm, this work suggests a procedure for the simultaneous in situ determination of the internal stresses in many bulk grains.

Acknowledgements

We thank our colleagues C. Klitholm and A. Goetz for preparing the stress-rig for operation at the beam line, E.M. Lauridsen and S. Schmidt for help with indexing the spots, U. Lienert for help with the synchrotron optics, P. Nielsen for sample preparation and Å. Kvick and his staff at ID11, ESRF, for general support. This work was supported by the Danish Natural Science Research Council via the Dansync Centre, and by the Danish Technical Research Council via its funding to the Engineering Science Centre for Structural Characterization and Modelling of Materials at Risø National Laboratory.

References

[1] Sachs G. Z verein deut Ing 1928;72:734.
[2] Taylor GI. J Inst Met 1938;62:307.
[3] Leffers T. Risø report no. 184. Roskilde: Risø National Laboratory, 1968.
[4] Mecking H. In: Haasen P, editor. Proceedings ICSMA 5, vol. 3. Oxford: Pergamon Press; 1980. p. 157-3.
[5] Kocks UF, Canova GR. In: Hansen N, editor. Deformation of polycrystals. Roskilde: Risø National Laboratory; 1981. p. 3-5.
[6] Kröner E. Acta Metall 1961;9:155.
[7] Hutchinson JW. Proc R Soc London 1970;A319:247.
[8] Tiem S, Berveiller M, Canova GR. Acta Metall 1986;34:2139.
[9] Molinari A, Canova GR, Ahzi S. Acta Metall 1987;35:2983.
[10] Lebensohn RA, Tomé CN. Acta Metall Mater 1993;41:2611.
[11] Kalidindi SR, Bronkhorst CA, Anand LJ. Mech Phys Solids 1992;40:537.
[12] Bronkhorst CA, Kalidindi SR, Anand L. Philos Trans R Soc London 1992;A341:443.
[13] Dawson PR, Beaudoin AD, Mathur KK. In: Andersen SI, editor. Numerical prediction of deformation processes and the behaviour of real materials. Roskilde: Risø National Laboratory; 1994. p. 33.
[14] Mika DP, Dawson PR. Mater Sci Eng 1998;A257:62.
[15] Berveiller M, Hihi A, Zaoui A. In: Hansen N, editor. Deformation of polycrystals. Roskilde: Risø National Laboratory; 1981. p. 14-5.
[16] MacEwen SR, Christodoulou N, Tomé C, Jackman J, Holden TM. In: Kallend JS, Gottstein G, editors. Proceedings ICOTOM 8. Warrendale: The Metallurgical Society; 1988. p. 82-5.
[17] Clausen B, Lorentzen T, Leffers T. Acta Mater 1998;46:3087.
[18] Dawson PR, Boyce D, MacEwan S, Rogge R. Metall Mater Trans 2000;31A:1543.
[19] Holden TM, Bowen AW. In: Hutchins MT, Krawitz AD, editors. Measurement of residual and applied stress using neutron diffraction. Dordrecht: Kluwer Academic Publishers; 1992. p. 22-3.

[20] Lorentzen T. Introduction to characterization of residual stress by neutron diffraction, 1st ed. Gordon and Breach Science Publishers, 2001.
[21] Hutchings MT, Krawitz AD, editors. Measurement of residual and applied stress using neutron diffraction. Dordrecht: Kluwer Academic Publishers; 1992.
[22] Kalidindi SR, Bronkhorst CA, Anand L. J Mech Phys Solids 1992;40:537.
[23] Poulsen HF, Garbe S, Lorentzen T, Juul Jensen D, Poulsen FW, Andersen NH et al. J Synchrotron Rad 1997;4:147.
[24] Lienert U, Poulsen HF, Kvick A. In: Proceedings of the 40th Conference of AIAA: Structures, structural dynamics and materials, St Louis, USA. 1999. p. 206-7.
[25] Juul Jensen D, Kvick A, Lauridsen EM, Lienert U, Margulies L, Nielsen SF et al. Mater Res Soc Symp Proc 2000;590:227.
[26] Lauridsen EM, Schmidt S, Poulsen HF, Suter RM. J Appl Crystallogr 2001;34(6):744–50.
[27] Poulsen HF, Nielsen SF, Lauridsen EM, Schmidt S, Suter RM, Lienert U et al. J Appl Crystallogr 2001;34(6):751–6.
[28] Nielsen SF, Ludwig W, Bellet D, Lauridsen EM, Poulsen HF, Juul Jensen D. In: Hansen N, editor. Proceedings of the 21st Risø International Symposium on Materials Science. Denmark: Risoe National Laboratory; 2000. p. 473–8.
[29] Margulies L, Winther G, Poulsen HF. Science 2001;291:2392–4.
[30] Hammersley AP, Svensson SO, Thompson A. Nucl Instrum Methods 1994;A346:312.
[31] Press HW, Teukolsky AA, Vetterling WT, Flannery BP. Numerical recipes in FORTRAN: The art of scientific computing, 2nd ed. Cambridge University Press, 1992.